Hydrology and Earth System Sciences, 4(3), *393–405* (2000) © EGS

Hydrology & Earth System Sciences

Flood frequency estimation by continuous simulation under climate change (with uncertainty)

David Cameron[1], Keith Beven[1] and Pamela Naden[2]

[1]Institute of Environmental and Natural Sciences, Lancaster University, Lancaster, LA1 4YQ, UK
[2]Centre for Ecology and Hydrology, Crowmarsh Gifford, Wallingford, Oxfordshire, OX10 8BB, UK
e-mail for corresponding author: david.cameron@environment-agency.gov.uk

Abstract

This paper explores the potential for assessing the impacts of climate change upon flood frequency for the gauged, upland Wye catchment at Plynlimon, Wales, UK, while taking account of uncertainty in modelling rainfall-runoff processes under current conditions. A continuous simulation methodology which uses a stochastic rainfall model to drive the rainfall-runoff model TOPMODEL is utilised. *Behavioural* parameter sets for both the rainfall model and TOPMODEL are identified prior to the climate change runs using the Generalised Likelihood Uncertainty Estimation (GLUE) methodology. The "medium-high" UKCIP98 climate change scenario, obtained from the HadCM2 GCM simulations, is used as a starting point for a variety of different scenarios at the catchment scale. It is demonstrated that while the scenarios have only a small impact upon the likelihood weighted flood frequency uncertainty bounds in comparison with the current condition scenario, the risk of a given discharge as an element in the distribution of T year floods is changed. This underlines the need to account explicitly for uncertainty within hydrological modelling, especially in estimating the impacts of climate change.

Keywords: Climate change; Floods; Frequency; TOPMODEL

Introduction

One of the key assumptions of flood frequency analysis is that the return period of a flood peak of given magnitude is stationary with time (e.g. NERC, 1975). This assumption is only valid if a catchment's long-term climatic, physical and hydrological characteristics are also relatively constant with time. Recent studies (e.g. Wigley and Raper, 1992; Arnell and Reynard, 1996; Hulme and Jenkins, 1998; Pilling *et al.*, 1998; Hulme *et al.*, 1999), however, have demonstrated the variability of climate characteristics and the potential for hydrological impacts of future climate change. The UK Climate Impacts Programme (e.g. UKCIP98, Hulme and Jenkins, 1998), for example, derived several possible climate change scenarios for the UK in the 21st Century using output from the Hadley Centre global climate model (or GCM), HadCM2. These scenarios included changes to precipitation and evapotranspiration.

These changes may have serious implications for flood frequency (e.g. Lettenmaier and Gan, 1990; Beven, 1993a; Naden *et al.*, 1996; Panagoulia and Dimou, 1997; Gellens and Roulin, 1998). If so, then there is a clear need to estimate the impacts of climate change upon flood frequency. This is a complex problem. A GCM is subject to large uncertainties in its representation of the current climate at regional, and smaller, scales (especially with respect to rainfall). In addition, a GCM's economic and computational cost also often prohibits the number of multiple runs which can be made. Thus, it is not currently possible to assign specific probabilities to climate change predictions. The predictions must rather be evaluated as potential scenarios that are dependent on assumptions of future greenhouse gas inputs and current GCM modelling technology. This situation is further complicated by the choice of GCM (different models may yield different results, e.g. Kattenberg *et al.*, 1998) and the large spatial and temporal scales at which GCMs operate. HadCM2, for example, utilises gridboxes of the order of 250 km in size, with estimated changes to climate variables (such as rainfall) being stored at a monthly timescale for each gridbox (Hulme and Jenkins, 1998).

The use of GCM output with a rainfall-runoff model (e.g. for the purpose of flood frequency estimation by continuous simulation at the catchment level) therefore normally requires some form of spatial downscaling (Bloschl and Sivapalan, 1995; Hulme and Jenkins, 1998; Kilsby *et al.*, 1998). This can be subject to large errors, especially with respect to rainfall (e.g. Pilling *et al.*, 1998). In addition, a decision as to how to apply the estimated monthly changes at the smaller timesteps required by the rainfall-runoff model (e.g. the hourly timestep used by Blazkova and Beven, 1997) must also be made.

In a previous study, Wolock and Hornberger (1991) used a stochastic rainfall model, together with the rainfall-runoff model TOPMODEL (Beven *et al.*, 1995; Beven, 1997, 2000) and a temperature and potential evapotranspiration model, in order to investigate the effects of climate change upon the hydrology of the White Oak Run catchment, Virginia, USA. It was demonstrated that there was considerable uncertainty associated with the magnitudes and directions of the resulting changes in the catchment's hydrological characteristics when multiple realisations of different climate change scenarios were simulated.

In what follows, the continuous simulation methodology developed by Cameron *et al.* (1999) is used to investigate the impacts of climate change upon flood frequency for a gauged, upland catchment in the UK. This features the use of TOPMODEL together with a stochastic rainfall model, under the Generalised Likelihood Uncertainty Estimation (GLUE) framework (Beven and Binley, 1992). Several different implementations of HadCM2 climate change scenarios at the catchment scale are considered. Uncertainties involved in the estimations are highlighted and the practical implications for flood management and engineering design are discussed.

The study site

The 10.6 km^2 Wye catchment at Plynlimon, Wales, UK, was selected as a study site (Fig. 1). This catchment possesses an upland terrain consisting of a high relief of weathering resistant slates and shales, overlain by peat and grassland. Both rainfall and runoff are fairly high (approximately 2457 mm $year^{-1}$, and 2075 mm $year^{-1}$, respectively). The mean annual flood is 19.2 m^3s^{-1}, while the flow duration curve exhibits Q50, Q75 and Q95 values of 0.360 m^3s^{-1}, 0.178 m^3s^{-1} and 0.070 m^3s^{-1}. Pipeflow is known to occur within the soils (Kirby *et al.*, 1991; Sklash *et al.*, 1996). The catchment is therefore very responsive to storm rainfalls.

The Wye has been one of the Centre for Ecology and Hydrology's major experimental catchments since 1968 (e.g. Kirby *et al.*, 1991). A large data set is therefore available. This includes 21 years (1969-1989) of hourly flow and catchment average hourly rainfall data (or CAHR), derived from a network of 21 gauges. Nineteen years of MORECS (Thompson *et al.*, 1981) monthly potential evapotranspiration data are also available for the 40 km square in which the Wye catchment lies. These data have been temporally disaggregated to a daily level according to the pattern of daily potential evapotranspiration estimates for 1988 for the MORECS synoptic site at Ludlow College, England, UK.

This large data set for the Wye catchment has formed the basis for many previous modelling studies. These have included the use of both physically-based, distributed models (such as the IHDM e.g. Morris, 1980; Binley *et al.*, 1991; and SHE e.g. Bathurst, 1986) and simpler, semi-distributed models (notably TOPMODEL e.g. Beven, 1987; Quinn and Beven, 1993). For computational reasons, flood frequency studies have employed the latter simpler model types in order to simulate the catchment response. In the studies of Beven (1987) and Cameron *et al.* (1999), a stochastic rainfall generator was used in conjunction with TOPMODEL to generate one hundred and one thousand year simulations with an hourly timestep, respectively.

Many previous climate change impact studies (e.g. Naden *et al.*, 1996; Kilsby *et al.*, 1998) have been conducted at regional or large catchment scales (typically ranging from hundreds to thousands of km^2 with respect to catchment area) but without any consideration of the uncertainty in the predictions arising from the uncertainty in modelling the rainfall-runoff process. The results presented in this paper therefore demonstrate a new direction for climate change impact studies at the local scale for a gauged catchment (climate change studies at ungauged sites would be subject to further uncertainties, Calver *et al.*, 1999).

The hydrological model

Full details of TOPMODEL may be found in Beven *et al.* (1995), and Beven (1997, 2000), so only a brief summary is outlined here.

TOPMODEL is a simple semi-distributed model of

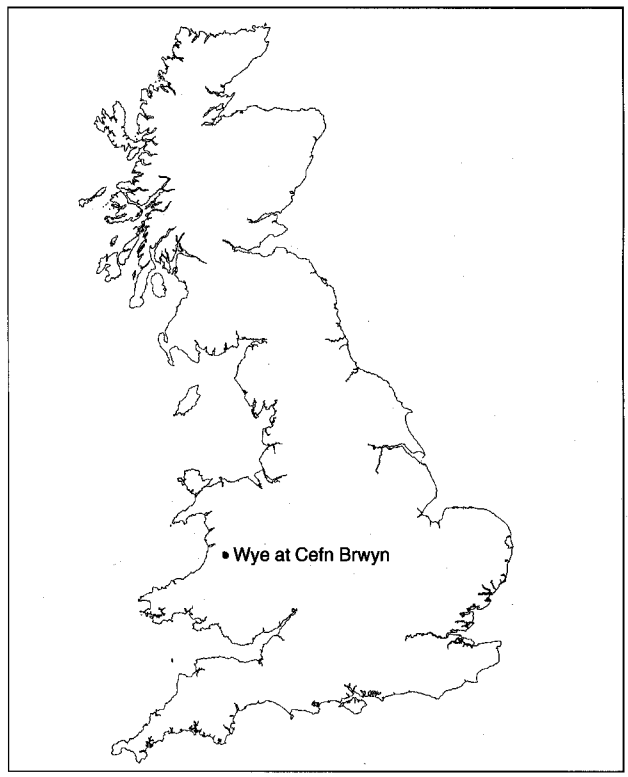

Fig. 1. *The location of the Wye catchment.*

catchment hydrology that estimates storm runoff from a combination of variable saturated surface contributing area and subsurface runoff (e.g. Beven 1986, 1987; Quinn and Beven, 1993). The dynamics of the contributing area for rapid runoff as the catchment wets and dries are based on a quasi-steady state analysis. As with many other TOPMODEL applications (see Beven, 1997), the topographic index ln (a/tan β) is used as an index of hydrological similarity, where a is the area draining through a point, and tan β is the local surface slope. The use of this form of topographic index implies an effective transmissivity profile that declines exponentially with increasing storage deficits. In this study, the derivation of the topographic index from a catchment digital terrain model utilises a modified form of Quinn *et al.*'s (1991, 1995) multiple flow direction algorithm (see Cameron *et al.*, 1999).

Evapotranspiration losses are controlled by potential evapotranspiration and storage in the root zone with the parameter S_{rmax} (effective available water capacity at the root zone). The potential evapotranspiration estimation routine uses the same seasonal sine curve as Beven (1986, 1987) and Blazkova and Beven (1997) with a single mean hourly potential evapotranspiration (*PET*) parameter. This was derived from the available 19 years of daily potential evapotranspiration estimates.

In a previous study of the Wye by Cameron *et al.* (1999), it was shown that, when driven by the observed catchment average hourly rainfall (or CAHR), TOPMODEL could reproduce successfully the observed 21 year record of hourly annual maximum (ANNMAX) flood peaks. It was also demonstrated that it is possible to identify parameter sets which provide reasonable simulations of both the observed hourly ANNMAX flood frequency curve and the 21 year continuous hourly hydrograph. However, because of errors in the input rainfalls, observed discharge peaks and model structure, these hydrograph simulations are not always able to reproduce accurately the exact timings and rankings of the observed hourly flood peaks. Similar findings have also been made in other flood estimation studies (e.g. Lamb, 1999) and this suggests that this may be a generic problem in current hydrological modelling.

Further modelling of the ANNMAX flood peak record was achieved through the coupling of TOPMODEL with a stochastic rainfall model. This permitted multiple one thousand year continuous hourly discharge time series to be generated and analysed in order to estimate the probability distribution of the floods of a given magnitude. Here, this latter approach is utilised in order to investigate the impacts of climate change upon the hourly ANNMAX flood peaks of both short and long return period (e.g. 10 to 100 years).

The stochastic rainfall model

Full details of the development of the stochastic rainfall model and its application to the Wye's CAHR data are detailed in Cameron *et al.* (1999). In that study, it was shown that the model could satisfactorily reproduce the Wye's hourly and daily extreme rainfall amounts. An identical modelling approach is utilised here, so only a brief summary is provided.

The stochastic rainfall model is based upon the available data and generates random rainstorms via a Monte Carlo sampling procedure. The model characterises a storm in terms of a mean storm intensity, duration, inter-event arrival time and storm profile. A rainstorm is defined as any event with a minimum intensity of 0.1 mm at an hour, with a minimum duration of 1 hr and a minimum inter-event arrival time of 1 hr. This definition accounts for 99% of the rainfall data in the observed series.

It is assumed that mean storm intensity is dependent upon storm duration. This is modelled by subdividing the available observed sample of storm events (derived from the 21 year record of CAHR) into seven duration classes of similar mean storm intensity: 1 hr, 2 to 3 hr, 4 to 10 hr, 11 to 16 hr, 17 to 27 hr, 28 to 62 hr, and $\geq$63 hr. For each duration class, log-transformed mean storm intensity is modelled using the empirical cumulative density function (cdf) derived from the storm events located within that class.

In order to permit the generation of events unrecorded within the available catchment storm series, the upper tails of the cdfs are extrapolated via a Generalised Pareto distribution (GPD). The GPD has the distribution function:

$$\begin{aligned} F(x) &= 1 - (1 + [\kappa(x-u)/\sigma])^{-1/\kappa} \qquad \kappa \neq 0 \\ F(x) &= 1 - \exp[-(x-u)/\sigma] \qquad \kappa = 0 \end{aligned} \tag{1}$$

Where F(x) is a non-exceedance probability, κ is a shape parameter, u (the intensity threshold) is a location parameter, x-u is an exceedence (where $x > u$), and σ is a scale parameter.

This distribution is initially fitted using maximum likelihood. For the 1 hr, 2 to 3 hr and $\geq$63 hr duration class, an upper bound, based upon the maximum observed UK rainfalls, is introduced to the fit in order to prevent the generation of unrealistically high mean storm intensities (see Cameron *et al.*, 1999). It introduces a dependency between the shape (κ) and scale (σ) parameters of the GPD and therefore does not increase the number of parameters required.

The storm duration and inter-event arrival time characteristics derived from the observed event series are also modelled using their empirical cdfs. In both cases, it is assumed that the observed samples require no further extrapolation.

The final component of the model is a storm profile. The observed 21 year rainstorm event series (a total of 10058 events) is utilised to provide an extensive database of storm profiles for each duration class (Cameron *et al.*, 1999). These are normalised by cumulative volume and total

duration. During a model run, the normalised profiles are randomly selected in order to provide storm profiles for the simulated rainfall events.

The Generalised Likelihood Uncertainty Estimation (GLUE) framework

Every flood frequency estimate is subject to some degree of uncertainty. The major sources of this uncertainty in the continuous simulation approach include the limitations of the observed data series and the choice of rainfall and hydrological models (especially with respect to the model structures, and their calibration/validation). In this study, the Generalised Likelihood Uncertainty Estimation (GLUE) framework of Beven and Binley (1992) was used to assess the resulting uncertainty in the predictions (see also Beven, 1993b; Freer *et al.*, 1996; Franks *et al.*, 1998; Cameron *et al.*, 1999).

The GLUE methodology rejects the concept of a single, global optimum parameter set and instead accepts the existence of multiple acceptable (or *behavioural*) parameter sets (Beven, 1993b). In a previous study of the Wye catchment by Cameron *et al.* (1999), GLUE was used to identify one thousand *behavioural* TOPMODEL parameter sets and one thousand *behavioural* GPD parameter sets for each duration class of the rainfall model.

A TOPMODEL parameter set was defined as *behavioural* if it could produce adequate reproductions of both the Wye's observed hourly annual maximum flood frequency curve (as assessed via a log likelihood measure, $l(\rho)$) and the catchment's continuous 21 year continuous hourly hydrograph (as assessed via the Nash and Sutcliffe, 1970, efficiency with a minimum acceptability threshold of 70%) when TOPMODEL was driven by the observed rainfall series (see Cameron *et al.*, 1999). Within each parameter set, four TOPMODEL parameters had been sampled from separate uniform distributions prior to the evaluation. These are: the exponential scaling parameter (m), effective available water capacity of the root zone (S_{rmax}), mean log transmissivity of the soil at saturation of the surface ($\ln(T_0)$), and standard deviation of log transmissivity ($STDT$). Table 1 contains the *behavioural* ranges of these parameters.

A GPD parameter set was defined as *behavioural* if its fit to the upper tail of the mean storm intensity cdf of the duration class in question was acceptable (as assessed by a log likelihood measure, $l(\theta)$). An additional requirement was that that GPD fit did not exceed an assumed upper bound of rainfall intensity at levels of high non-exceedance probability (see Cameron *et al.*, 1999). Where the upper bound featured in the earlier maximum likelihood fit, σ was initially sampled from a uniform distribution and κ calculated. Otherwise, both parameters were initially sampled from separate uniform distributions. For each duration class,

Table 1. Parameter ranges of 1000 *behavioural* TOPMODEL parameter sets.

Parameter	Range
m (recession)	0.0089:0.0152 m
S_{rmax} (maximum root zone storage)	0.0016:0.1995 m
T_0 (transmissivity)	1.4403:7.9991 log
$STDT$ (standard deviation from transmissivity)	1.0048:9.1579 log

Table 2 contains the *behavioural* ranges of these parameters together with their maximum likelihood estimates.

The one thousand *behavioural* TOPMODEL and rainfall model parameter sets (combined randomly) were used to simulate separate one thousand year continuous hourly rainfall and discharge time-series. The hourly annual maximum (ANNMAX) flood peaks were extracted from each simulated discharge series. Likelihood weighted uncertainty bounds for flood frequency were then calculated. This calculation required the use of a combined measure (CM), which assumed equal weightings between the rainfall and TOPMODEL parameter sets. For the k th *behavioural* simulation, CM is defined as:

$$CM_k = \exp\{l(\rho)_k + 1/nd \cdot \sum_{i=1}^{nd} [l_s(\theta)_i]_k\} \qquad (2)$$

Where nd is the number of cdfs requiring extrapolation (seven), and $l_s(\theta)$ is the rescaling of each value of $l(\theta)$ such that they share a common scale with $l(\rho)$.

The CM likelihood weights were rescaled over all of the *behavioural* simulations in order to produce a cumulative sum of 1.0. A cdf of discharge estimates was constructed for each ANNMAX peak using the rescaled weights. Linear interpolation was used to extract the discharge estimate appropriate to cumulative likelihoods of 0.05, 0.5, and 0.95. This allowed 90% uncertainty bounds, in addition to a median simulation, to be derived (see also Freer *et al.*, 1996; Cameron *et al.*, 1999). The cumulative likelihood weighted distribution used in this procedure is calculated using:

$$P(Q_T < q) = \left[\sum_{k=1}^{ns} (CM_k / \sum_{k=1}^{ns} CM) | Q_{T,k} < q \right] \qquad (3)$$

Where P is a probability, Q is a discharge of T years return period, q is a discharge, and ns is the number of *behavioural* simulations.

In the present study, the one thousand *behavioural* TOPMODEL and rainfall model parameter sets, together with their original likelihood weightings, are used to produce a 1000 element series of 1000 year hourly rainfall and discharge time-series for several different climate change scenarios. Hourly ANNMAX flood frequency

Table 2. Maximum likelihood estimates and parameter ranges for the 1000 *behavioural* GPD parameter sets fitted to the log-transformed upper tails of the duration class mean storm intensities.

Class	No. Stm	Scale (σ)		Shape (k)	
		Max. Like. Estimate	Range	Max. Like. Estimate	Range
1hr	200	0.6016	0.5542 : 0.6546	−0.1244	−0.1146 : −0.1353
2–3hr	200	0.3772	0.3474 : 0.4104	−0.0925	−0.0852 : −0.1006
4–10hr	200	0.3584	0.3246 : 0.3939	−0.2588	−0.1955 : −0.3117
11–16hr	200	0.5633	0.5120 : 0.6190	−0.3512	−0.2905 : −0.4011
17–27hr	200	1.0244	0.9391 : 1.1186	−0.5651	−0.5091 : −0.6221
28–62hr	40	1.7265	1.3450 : 2.2138	−1.1299	−0.8759 : −1.4488
⩾63hr	25	0.2867	0.2119 : 0.3779	−0.0899	−0.0865 : −0.1543

likelihood weighted uncertainty bounds are then calculated for each scenario.

Climate change scenarios

The recent UKCIP98 "medium-high" climate change scenario available from the UK Hadley Centre experiments (HadCM2) was used in this study (Hulme and Jenkins, 1998; Hulme *et al.*, 1999). In this scenario, it is assumed that there is a compound 1% per annum increase in greenhouse gas concentration with no change in the concentration of sulphate aerosols. Since the results of the scenario may depend upon the point at which the increasing greenhouse gas concentrations are introduced, four ensemble HadCM2 runs were used (Hulme and Jenkins, 1998). With the exception of the point of initial greenhouse gas increase, the conditions surrounding these runs are identical. This includes the use of annual flux-correction that were necessary for this generation of GCM predictions. Since it is not currently possible to assign probabilities to climate change scenarios (Hulme and Jenkins, 1998), the climate change estimates from each run were assumed to have equal likelihoods. There does not appear to be any realistic alternative to this assumption at the current time. Every uncertain prediction in this study is therefore the response to a particular scenario provided by the HADCM2 simulations of future conditions. The uncertainties estimated under the GLUE methodology are due only to the uncertainty in simulating the rainfall-runoff process under current conditions. To our knowledge, however, this is the first time that such uncertainties have been assessed relative to the impact of predicted future change.

In this study, the climate change estimates from the "medium-high" scenario were obtained from the HadCM2 gridbox which contains the country of Wales, UK by averaging the results of the four available ensemble runs. Data for three 30 year timeslices were available. The timeslices are: the 2020s (2010-2039), the 2050s (2040-2069), and the 2080s (2070-2099). For all three of the timeslices, the data includes the estimated changes to monthly rainfall and annual potential evapotranspiration (Table 3). This data indicates that, from the 2020s through to the 2080s, there are estimated increases in winter monthly rainfall totals (in this case, September to April), and decreases in summer monthly rainfall totals (May to August). Annual potential evapotranspiration is also expected to increase.

Monthly potential evapotranspiration change estimates were also available for the 2050s timeslice only. In addition, the changes to monthly rainfall estimated from each of the four individual HadCM2 ensemble runs were available for all three timeslices. These data are very important to this study and will be given further consideration below.

The concepts of spatial and temporal downscaling are important issues in terms of using GCM output at the local scale (Beven, 1995; Bloschl and Sivapalan, 1995; Hulme and Jenkins, 1998; Pilling *et al.*, 1998). Given the uncertainties associated with both the GCM output and the spatial downscaling procedures, it was decided to use the estimated changes for the GCM grid box directly on the Wye catchment. This procedure assumes that the changes modelled at the grid box scale are applicable at the local, site specific, level. In order to implement the HadCM2 estimated changes to monthly rainfall at an hourly timescale, fifteen different climate change scenarios were generated (Table 4, where Scenario Z, "current conditions", is equivalent to the

Table 3. GCM estimated changes to monthly rainfall derived from the mean of four HadCM2 ensemble runs (ens. mean) and the minimum (min.) and maximum (max.) flood frequency increase scenarios for three thirty year timeslices. Estimated changes to annual potential evapotranspiration are only readily available for the former case.

	2020s			2050s			2080s		
	% Change			% Change			% Change		
	Ens. mean	Min.	Max.	Ens. mean	Min.	Max.	Ens. mean	Min.	Max.
January	2.78	3.30	3.52	4.51	5.50	5.49	6.19	10.77	10.98
February	4.57	0.00	6.42	7.43	−0.28	10.34	10.19	−0.84	20.67
March	1.52	−2.02	0.29	2.47	−3.19	0.58	3.38	−6.38	1.16
April	2.61	−1.84	5.15	4.25	−2.94	8.09	5.82	−5.88	16.54
May	−0.22	1.09	−0.36	−0.36	1.82	−0.72	−0.50	3.27	−1.45
June	−1.20	4.67	3.11	−1.94	7.39	5.06	−2.67	14.40	10.51
July	−5.77	−1.70	−2.98	−9.37	−2.98	−4.68	−12.85	−5.96	−9.36
August	−3.19	−4.21	−2.27	−5.19	−7.12	−3.88	−7.12	−13.92	−7.77
September	0.84	1.90	−0.27	1.36	4.34	−0.54	1.87	6.25	−0.82
October	2.07	−4.48	1.49	3.36	−7.21	2.49	4.61	−14.18	4.98
November	4.69	4.47	2.68	7.62	7.16	4.47	10.45	14.31	8.94
December	5.02	5.15	4.74	8.16	8.45	8.87	11.20	16.70	17.73
Annual potential evapotranspiration	0.86	n/a	n/a	1.99	n/a	n/a	3.58	n/a	n/a

results previously obtained using the historical record by Cameron *et al.*, 1999). This use of multiple scenarios permitted several different possible impacts of climate change upon flood frequency to be explored.

For each of the fifteen scenarios, a one thousand year continuous simulation with hourly timestep was made for each of the one thousand *behavioural* TOPMODEL and stochastic rainfall model parameter set combinations. The

Table 4. Summary of several possible climate change scenarios using HadCM2 estimated changes to monthly rainfalls – see text for details.

Scenario no.	Timeslice	Implementation of estimated monthly rainfall changes
Z	Current conditions	n/a
A1	2020s	Uniform
B1	2050s	Uniform
C1	2080s	Uniform
A2	2020s	Uniform minimum increase
A3	2020s	Uniform maximum increase
B2	2050s	Uniform minimum increase
B3	2050s	Uniform maximum increase
C2	2080s	Uniform minimum increase
C3	2080s	Uniform maximum increase
A4	2020s	Upper 10% of storms only
A5	2020s	Upper 50% of storms only
A6	2020s	Duration class 1 and 2 only
A7	2020s	Duration class 3 to 7 only
A8	2020s	Duration class 1 and 2 only if estimated increase, duration class 3 to 7 only if estimated decrease
A9	2020s	Shorter winter arrival times, uniform summer changes

likelihood weighted uncertainty bounds for the hourly ANNMAX flood peaks were then calculated (using the procedures outlined previously in this paper). With the exception of scenario A9, all of the scenarios featured the perturbation of an identical hourly rainfall series to that generated in scenario Z. This was done in order to prevent the possible impacts of climate change being confounded with random rainfall realisation.

In the above procedure there is an implicit assumption that the *behavioural* parameter sets and likelihood weights will not change under future conditions (and that only the model inputs will change). Again, there appears to be no other reasonably realistic assumption at the current time. It should also be remembered that the likelihood weights do reflect the catchment's responses under a wide range of conditions during the 21 year record.

In all fifteen scenarios, the impacts of climate change upon potential evapotranspiration were implemented through the perturbation of the *PET* parameter used in TOPMODEL. This perturbation was calculated prior to a model run, as:

$$PET_r = PET_i + (PET_i \cdot CHG/100) \qquad (4)$$

Where PET_r is the value of *PET* used in a model run, PET_i is the value of *PET* calculated from the 19 years of daily potential evapotranspiration estimates (0.05830 mm hr^{-1}), and *CHG* is the change estimated by HadCM2.

For the 2050s timeslice, an examination of the implications of the choice of potential evapotranspiration change estimates (i.e. monthly or annual) for the simulated hourly annual maximum flood peaks was conducted. This examination consisted of the simulation of a 1000 element 1000 year continuous hourly discharge time-series (as described above). Monthly estimated changes to potential evapotranspiration were initially used. Perturbation of the simulated hourly rainfall amounts for a given month was achieved through the uniform application of the HadCM2-estimated change for that month (Table 3). The procedure was then repeated using the estimated changes to annual potential evapotranspiration. The resulting 5%, 50%, and 95% likelihood weighted uncertainty bounds calculated from the hourly annual maximum flood peaks simulated under each potential evapotranspiration regime were then compared. It was determined that there were only negligible differences between the two sets of results at the 10 year and 100 year return period levels. For consistency between the three timeslices, the estimated changes to annual potential evapotranspiration (Table 3) were therefore used in each case.

For each of the three timeslices, the estimated change in rainfall total for a given month was initially preserved through the uniform application of the change to every hourly rainfall value in that month. Primarily, this was achieved through the direct use of the averaged "medium-high" UKCIP98 scenario (scenarios A1, B1, and C1 in Table 4). In addition, since the "medium-high" scenario's component ensemble runs can be assumed to have equal likelihoods (see above), the climate change estimates obtained from each of those runs were examined. This was done in order to ascertain which of the individual runs would drive the maximum, and the minimum, increases to the magnitude of the simulated ANNMAX hourly flood peaks.

This involved the testing of the changes estimated by each ensemble run upon the different continuous hourly one thousand year rainfall-runoff simulations. The lack of potential evapotranspiration change data for these individual ensemble runs necessitated the use of the estimated change to annual potential evapotranspiration obtained from the ensemble mean (Table 3). Given the very wet and flashy nature of the Wye catchment, it is unlikely that this data restriction has a substantial impact upon the simulations of the hourly annual maximum flood peaks. Table 3 contains the changes to monthly rainfall from the identified "minimum" and "maximum" ensemble runs, respectively. These runs form the basis of scenarios A2 to A3, B2 to B3, and C2 to C3 (see Table 4).

A further exploration of the different implementations of the estimated monthly rainfall changes at the hourly level was also conducted. This featured the direct use of the "medium-high" UKCIP98 scenario for the 2020s timeslice (Table 3). Several sub-scenarios were examined (Table 4). These included the application of the changes to the storms with the most intense hourly rainfall values alone (scenarios A4 and A5), and also to the storms belonging to particular rainfall model duration classes (scenarios A6 to A8). For the appropriate storms in these scenarios, the estimated changes were applied in a proportional fashion. The most intense hourly rainfall value in a given storm was therefore subject to the largest absolute change.

In scenario A9, the increased monthly rainfall totals for winter were achieved by increasing the frequency of the winter storm events. This involved the setting of an upper bound upon the storm inter-arrival times for each winter month (Table 5). This was achieved through multiple realisations using the stochastic rainfall model (with no GPD extrapolation). Each realisation was assigned an upper inter-event arrival time limit for a particular month, and the results compared with those of an initial control run. For a given month, if the change in the monthly rainfall total approximately corresponded to that estimated by HadCM2, then the limit was retained. The resulting bounds are therefore not absolute, but serve as a useful guide for exploring the estimated increase in the frequency of winter rainfall in a way which is consistent with the HadCM2 simulations.

It was also originally intended to reduce the storm numbers in the summer months through the setting of a lower bound upon inter-arrival time. However, it was found that, for this very wet catchment, even small increases in summer storm inter-event arrival time resulted in decreases

Table 5. Approximate upper limits for winter arrival-times in order to preserve HadCM2 estimated monthly rainfall changes for the 2020s.

Month	Limit upon storm inter-arrival time (hrs)
January	171
February	82
March	129
April	177
May	n/a
June	n/a
July	n/a
August	n/a
September	139
October	168
November	145
December	194

in the corresponding monthly rainfall totals which were much larger than those of the HadCM2 estimates. One possible solution to this problem would be to set an assumed lower bound and modify the intensities of the summer storms such that the monthly rainfall totals of the simulations are consistent with the HadCM2 estimates. However, it was felt that this approach would not be entirely in keeping with the method used for the winter storms (since only the frequencies, and not the intensities, of those storms were modified). Furthermore, it is probable that the setting of a lower bound in such a manner would be quite arbitrary. In addition, a choice of procedure for rainfall intensity modification would be required. Consequently, for reasons of simplicity, the uniform application of change used in scenario A1 was also adopted for the summer period.

Results and discussion

For each of the scenarios outlined in Table 4, Table 6 contains the hourly discharge estimates for the 10 and 100 year return period ANNMAX flood events at the 5%, median, and 95% likelihood weighted uncertainty levels. These are also expressed as percentage changes from scenario Z. Table 7 lists the ranges of the future return periods estimated for the median modelled flood peaks which have recurrence intervals of 10 and 100 years under scenario Z.

From these tables, it can be seen that, with the exception of the scenarios for the 2080s (C1 to C3), the changes in flood peak discharge are generally relatively small. Indeed, the 10 and 100 year recurrence interval flood events modelled for scenario Z lie within the range of peak flows estimated for the same return periods for the 2020s and the 2050s (Table 7). The larger increases in flood magnitude and frequency estimated for the 2080s can be explained by HadCM2's simulation of greater amounts of winter rainfall for that timeslice than for the 2020s or the 2050s (Table 3).

It is also possible to examine these results visually. Figures 2a to 2c illustrate a comparison of the likelihood weighted uncertainty bounds derived from scenarios A1, B1 and C1 with those obtained from scenario Z. Figure 3 illustrates the cdfs calculated using the scaled likelihood weights and discharge estimates for the 100 year return period flood event of scenarios Z, A1, B1 and C1. From these figures, it can be seen that, although flood event magnitude does tend to increase following climate change (e.g. note the 2080s 95% uncertainty bound on Fig. 2c), there is a considerable degree of overlap in the uncertainties associated with all four scenarios.

A further indication of the spread of these uncertainties can be obtained by considering the maximum and minimum increase scenarios A2, A3, B2, B3, C2, and C3. From Table 6, two main findings are apparent. Firstly, although the maximum and minimum increase scenarios generally yield respectively greater and smaller increases to flood peak magnitude than those estimated in scenarios A1, B1 and C1, there are certain instances where this is not the case.

For example, the magnitude of the 100 year return period event is estimated to increase by 2.62% on the 5% uncertainty bound of scenario A1, but only by 1.21% at the same level under scenario A3. This slight discrepancy can be explained by the use of the individual ensemble run data, rather than the ensemble average (Table 3), in the maximum and minimum increase scenarios. Consequently, the ensemble average data occasionally estimate greater changes to the monthly rainfall totals than those estimated by the separate component ensemble runs (e.g. November for the 2050s, Table 3).

Secondly, flood peak magnitudes are reduced in certain of the minimum increase scenarios (e.g. a decrease of −2.03% in the magnitude of the 10 year return period event on the 95% uncertainty bound, Table 6). This is caused by the large decreases in summer rainfall estimated by the ensemble run used in these scenarios (Table 3).

Surprisingly, in scenario A4 (Table 6), the application of change to the upper 10% of the storms only, also has the effect of decreasing, rather than increasing, the magnitude of the simulated flood peaks. This finding also applies to scenarios A5 to A8, and to a lesser extent, to A9. This occurs because the reduction in summer rainfall partially reduces the quantity of antecedent soil moisture available for the early winter flood events. This rainfall reduction also suppresses the magnitude of what were ANNMAX summer flood peaks in scenario Z (it should be remembered that identical rainfall sequences were used for scenario Z and scenarios A1 to A8). Consequently, these peaks are replaced in the overall ANNMAX series by winter events. Although these events are enhanced, they do not quite equal the magnitude of the previous peaks and the overall ANNMAX peak magnitudes drop slightly. While a different rainfall

Table 6. Discharge estimates (Q Est.) of the 10 and 100 year return period flood events at the 5%, 50% and 95% levels based on the GLUE analysis. Percentage changes (% chg.) from the estimates obtained from scenario Z (current conditions) are also supplied.

Scenario no.	10 Year Return Period Event						100 Year Return Period Event					
	5% Q Est. (m^3s^{-1})	% chg	50% Q Est. (m^3s^{-1})	% chg	95% Q Est. (m^3s^{-1})	% chg	5% Q Est. (m^3s^{-1})	% chg	50% Q Est. (m^3s^{-1})	% chg	95% Q Est. (m^3s^{-1})	% chg
Z	28.07	n/a	33.45	n/a	39.47	n/a	42.04	n/a	51.92	n/a	66.14	n/a
A1	28.78	2.53	34.30	2.54	40.29	2.08	43.14	2.62	53.42	2.89	67.76	2.45
B1	29.41	4.77	34.91	4.36	41.04	3.98	44.16	5.04	54.54	5.05	69.42	4.96
C1	30.01	6.91	35.59	6.40	41.87	6.08	45.46	8.14	56.01	7.88	70.91	7.21
A2	28.79	2.57	33.42	−0.09	38.67	−2.03	42.55	1.21	51.46	−0.89	64.60	−2.33
A3	29.53	5.20	34.02	1.70	39.47	0.00	43.71	1.21	52.62	1.35	66.20	0.09
B2	29.15	3.85	33.87	1.26	39.27	−0.51	43.26	2.90	52.46	1.04	65.99	−0.23
B3	30.30	7.94	34.91	4.37	40.60	2.86	45.32	7.80	54.12	4.23	68.21	3.13
C2	30.51	8.69	35.28	5.47	40.94	3.72	46.37	10.30	55.61	7.11	70.56	6.69
C3	32.26	14.93	37.40	11.80	43.80	10.97	49.20	17.03	58.71	13.08	75.33	13.89
A4	27.59	−1.71	31.91	−4.60	36.90	−6.51	41.00	−2.47	49.95	−3.79	62.38	−5.68
A5	27.43	−2.28	31.54	−5.71	36.40	−7.78	40.61	−3.40	49.14	−5.35	61.56	−6.92
A6	27.31	−2.71	31.47	−5.92	36.18	−8.34	40.67	−3.26	48.95	−5.72	61.29	−7.33
A7	27.45	−2.21	31.55	−5.68	36.37	−7.85	40.63	−3.35	49.32	−5.01	61.79	−6.58
A8	27.35	−2.60	31.40	−6.13	36.12	−8.49	40.66	−3.28	48.84	−5.93	61.27	−7.36
A9	28.22	0.53	33.34	−0.33	39.30	−0.43	42.15	0.26	51.27	−1.25	65.56	−0.88

Table 7. Estimated future ranges of return periods for the median ANNMAX flood event discharges associated with the 10 and 100 year recurrence interval events of scenario Z.

Timeslice	Estimated future return period range for current 10 year recurrence event (yrs)	Estimated future return period range for current 100 year recurrence event (yrs)
2020s	8 to 11	86 to 132
2050s	8 to 10	86 to 100
2080s	6 to 8	48 to 60

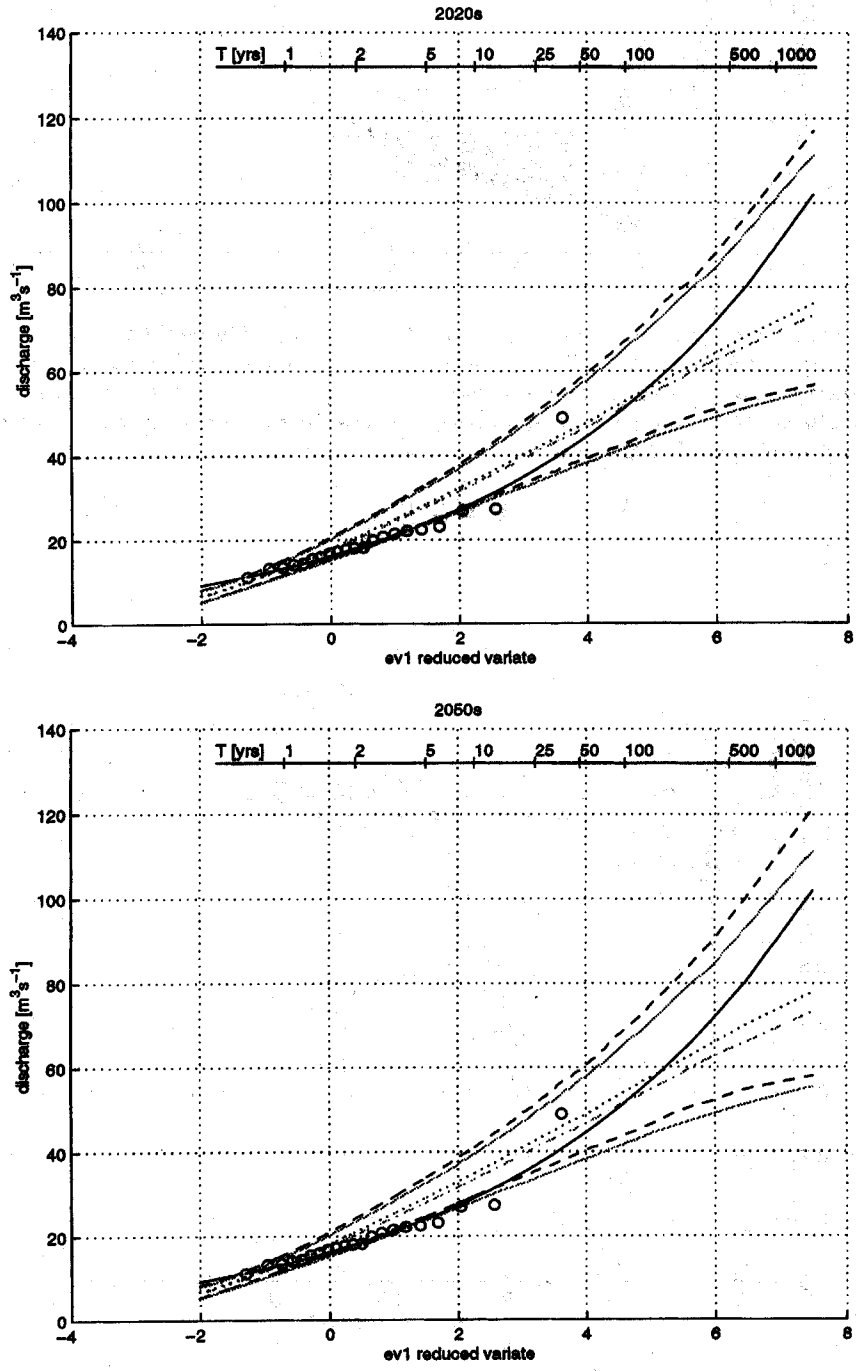

Fig. 2. *(continued over).*

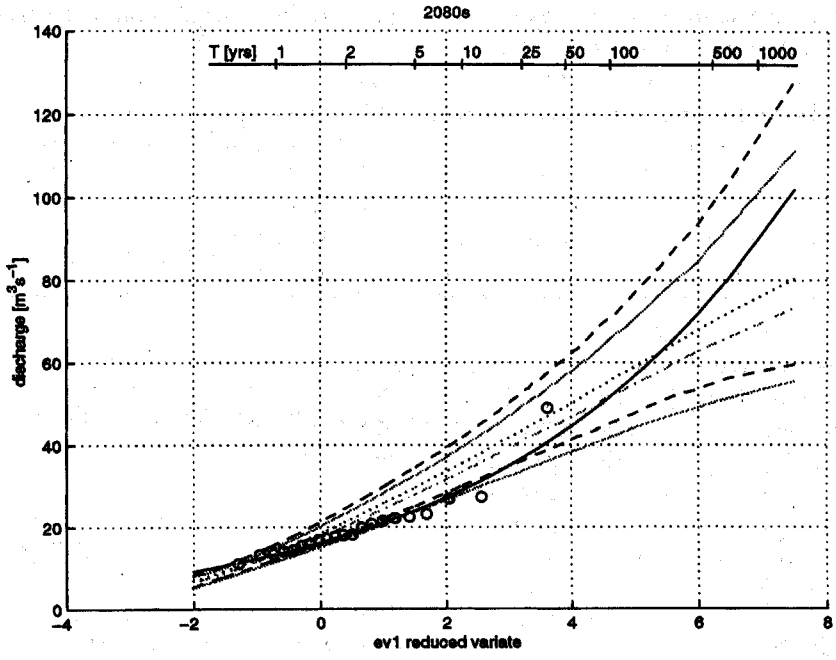

Fig. 2. *90% uncertainty bounds derived from annual maximum peaks of 1000 behavioural TOPMODEL/rainfall parameter sets with 1000 year simulation length. Circles–observed hourly peaks; dark solid line–observed series with fitted GEV (maximum likelihood); dashed lines–90% uncertainty bounds obtained from climate change scenarios; dotted line – median simulation obtained from climate change scenarios; light solid lines–90% uncertainty bounds obtained for scenario Z (current conditions); light dash-dot line–median simulation obtained for scenario Z. A: 2020s (scenario A1); B: 2050s (scenario B1); C: 2080s (scenario C1).*

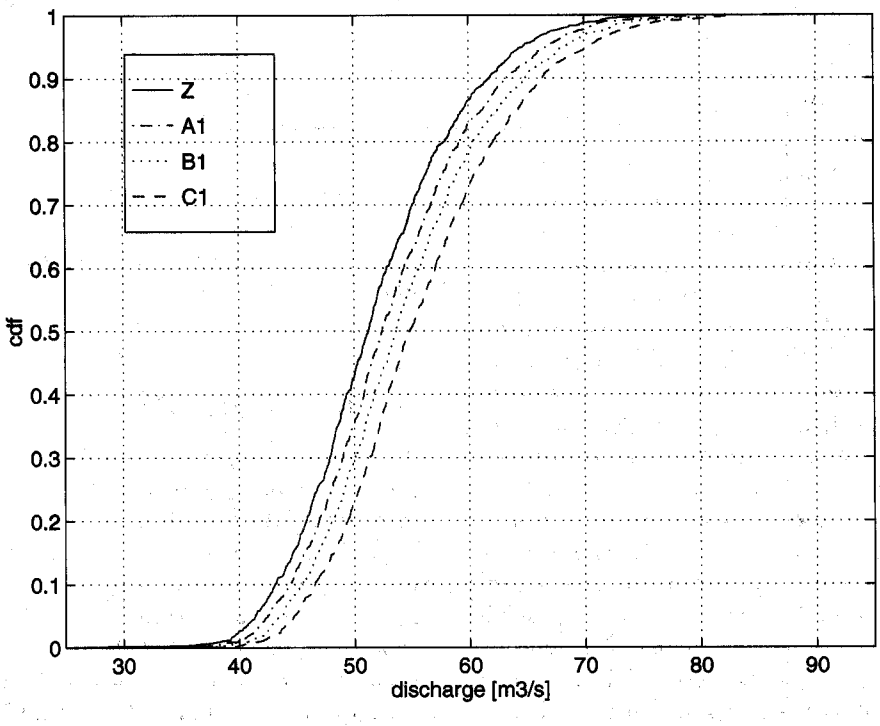

Fig. 3. *Cumulative density functions calculated using scaled likelihood weights and discharge estimates for the 100 year return period flood event of scenarios Z, A1, B1 and C1.*

sequence will yield different results (e.g. a possible increase, rather than a decrease), it is very probable that, given the results of scenarios A1 to A3, B2 to B3 and C2 to C3, the size of the change would only be large for the 2080s timeslice. It is likely that this magnitude of change also applies to the alterations to the winter storm inter-event arrival times modelled in scenario A9.

Since no probabilities can be currently assigned to different climate change scenarios, this study's overall results therefore suggest that, although there appears to be a general tendency for flood frequency to increase as a result of climate change, it may instead decrease or perhaps not change at all! In other words, given the choice of catchment and scenario, climate change generally appears to have only a small effect upon flood frequency when the uncertainties associated with the original observed data series, and hydrological model structure, are considered explicitly.

Indeed, it is interesting to note that other climate change rainfall-runoff modelling studies (e.g. Naden *et al.*, 1996; Kilsby *et al.*, 1998) have estimated larger impacts upon flood frequency than those presented in this paper. For the 2050s, Naden *et al.* (1996) report a 13.7% increase in the magnitude of the daily peaks over threshold 10 year flood event for the River Severn (a value comparable to the present study's results for the 2080s). For the 2080s, Kilsby *et al.* (1998) estimate very large increases (e.g. 60%) in daily ANNMAX flood magnitude for the Cobres basin, Portugal. The differences in the sizes of the changes estimated in these studies, compared with those of the present paper, can perhaps be attributed to the different choice of catchment environment, model, timestep, and downscaling and flood frequency procedures used in each case. However, both Naden *et al.* (1996) and Kilsby *et al.* (1998), utilised a rainfall-runoff model with a single optimal parameter set and made no explicit attempt to account for the associated modelling uncertainties.

Finally, from a flood management perspective, there is a clear need to have reliable flood frequency estimates both with and without climate change. In this context it is important to recognise that, although the form of discharge cdf for a given return period is not greatly changed relative to the uncertainty in predicting current conditions (e.g. Fig. 3), the risk of a given discharge as an element in the distribution of T year floods does change. For example, at a return period of 100 years, the risk of a 51.92 m^3s^{-1} event that is estimated at 0.5 under current conditions changes to 0.62 by the year 2050 under scenario B1. From the findings obtained in this study, it would seem that some form of uncertainty estimation (such as the GLUE framework presented) must be used if a proper assessment of flood frequency within a risk-based decision framework is to be achieved. It should then be possible to make more effective management and engineering decisions. These include: enhanced cost-benefit analysis and decision making for flood defence schemes, more robust flood defence designs, the continual assessment of their effectiveness, and increased public and professional awareness (Naden *et al.*, 1996).

Conclusions

This paper has explored explicitly the uncertainties associated with the impacts of climate change upon flood frequency for a gauged, upland catchment in the UK. It has featured the use of the continuous simulation methodology developed by Cameron *et al.* (1999). The methodology utilises a stochastic rainfall model to drive the rainfall-runoff model TOPMODEL for a series of continuous 1000 year simulations with hourly timestep. The uncertainty in the resulting hourly annual maximum flood peaks is handled within the GLUE framework of Beven and Binley (1992).

The "medium-high" UKCIP98 climate change scenario, obtained from the HadCM2 GCM (Hulme and Jenkins, 1998) was used as a starting point for a variety of different scenarios at the catchment scale. These featured the different applications of the changes to the monthly rainfall totals estimated by HadCM2 to the hourly level. The scenarios comprised: uniform changes to hourly rainfall for three 30 year timeslices (the 2020s, the 2050s and the 2080s), including those estimated from four different ensemble runs of HadCM2, changes to the hourly rainfalls of the most extreme storms and particular stochastic rainfall model duration classes only, and increases to the number of winter storm events. The estimated changes to annual potential evapotranspiration were used to perturb the parameter of the potential evapotranspiration model used by TOPMODEL.

It was demonstrated that while the scenarios have only a small impact upon the likelihood weighted flood frequency uncertainty bounds in comparison with the current condition scenario, the risk of a given discharge as an element in the distribution of T year floods is changed. This underlines the need to account explicitly for uncertainty within hydrological modelling, especially in estimating the impacts of climate change.

Acknowledgements

The authors wish to thank Nick Reynard for initial preparation of the climate change data. The HadCM2 output was made available through the Climate Impacts LINK project, funded by the Department of the Environment, Transport and the Regions, and based at the Climate Research Unit at Norwich, UK. The comments of an anonymous referee helped clarify areas of the paper. David Cameron's contribution to this work was carried out under the NERC CASE studentship GT4/97/112/F. The views of the first author do not necessarily represent those of the Environment Agency.

References

Arnell, N.W. and Reynard, N.S., 1996. The effects of climate change due to global warming on river flows in Great Britain, *J. Hydrol.* **183**, 397–424.

Bathurst, J.C., 1986. Physically-based distributed modelling of an upland catchment using the Systeme Hydrologique Europeen, *J. Hydrol.*, **87**, 103–123.

Beven, K., 1986. Hillslope runoff processes and flood frequency characteristics, in A.D. Abrahams (Ed), *Hillslope Processes*, 187–202, Allen and Unwin.

Beven, K., 1987. Towards the use of catchment geomorphology in flood frequency predictions, *Earth Surf. Proc.* **12**, 69–82.

Beven, K.J., 1993a. Riverine flooding in a warmer Britain, *Geograph. J.* **159**, 157–161.

Beven, K.J., 1993b. Prophecy, reality and uncertainty in distributed hydrological modelling, *Adv. in Water Resour.* **16**, 41–51.

Beven, K.J. (Editor), 1997. *Distributed modelling in hydrology: applications of the TOPMODEL concepts*, Wiley, Chichester, UK.

Beven, K.J., 2000. *Rainfall-runoff modelling – the primer*, Wiley, Chichester, UK.

Beven, K.J. and Binley, A., 1992. The future of distributed models: model calibration and uncertainty prediction, *Hydrol Process.* **6**, 279–298.

Beven, K., Lamb, R., Quinn, P., Romanowicz, R., and Freer, J., 1995. TOPMODEL, in V.P. Singh (Ed), *Computer Models Of Watershed Hydrology* 627–668, Water Resources Publications.

Binley, A.M., Beven, K.J., Calver, A. and Watts, L.G., 1991. Changing responses in hydrology: assessing the uncertainty in physically based model predictions, *Water Resour. Res.* **27**, 1253–1261.

Blazkova, S and Beven, K.J., 1997. Flood frequency prediction for data limited catchments in the Czech Republic using a stochastic rainfall model and TOPMODEL, *J. Hydrol.* **195**, 256–278.

Bloschl, G. and Sivapalan, M., 1995. Scale issues in hydrological modelling: a review, *Hydrol. Process.* **9**, 251–290.

Calver, A., Lamb, R. and Morris, S., 1999. River flood frequency estimation using continuous runoff modelling. *Proc. Instn. Civ. Engrs Water, Maritime & Energy*, **136**, 225–234.

Cameron, D.S., Beven, K.J., Tawn, J., Blazkova, S. and Naden, P., 1999. Flood frequency estimation for a gauged upland catchment (with uncertainty), *J. Hydrol.* **219**, 169–187.

Franks, S.W., Gineste, P., Beven, K.J. and Merot, P., 1998. On constraining the predictions of a distributed model: the incorporation of fuzzy estimates of saturated areas into the calibration process, *Water Resour. Res.* **34**, 787–798.

Freer, J., Beven, K. and Ambroise, B., 1996. Bayesian uncertainty in runoff prediction and the value of data: an application of the glue approach, *Water Resour. Res.* **32**, 2163–2173.

Gellens, D. and Roulin, E., 1998. Streamflow response of Belgian catchments to IPCC climate change scenarios, *J. Hydrol.* **210**, 242–258.

Hudson, J.A., Crane, S.B. and Blackie, J.R., 1997. The Plynlimon water balance 1969-1995: the impact of forest and moorland vegetation on evaporation and streamflow in upland catchments, *Hydrol. Earth Syst. Sci.* **1**, 409–427.

Hulme, M. and Jenkins, G.J., 1998. *Climate change scenarios for the UK: scientific report, UKCIP Technical Report No. 1*, Climate Research Unit, Norwich.

Hulme, M., Barrow, E.M., Arnell, N.W., Harrison, P.A., Johns, T.C., and Downing, T.E., 1999. Relative impacts of human-induced climate change and natural climate variability, *Nature* **397**, 689–691.

Kattenberg, A., Giorgi, F., Grassl, H., Meehl, G.A., Mitchell, J.F.B., Stouffer, R.J., Tokioka, T., Weaver, A.J. and Wigley, T.M.L, 1996. Climate models–projections of future climate, in J.T. Houghton, L.G. Meiro Filho, B.A. Callendar, N. Harris, A. Kattenberg and K. Maskell (eds) *Climate Change 1995: the science of climate change change*, 285–358, Cambridge University Press.

Kilsby, C.G., Fallows, C.S., and O'Connell, P.E., 1998. Generating rainfall scenarios for hydrological impact modelling, in: H. Wheater and C. Kirby (eds), *Hydrology In A Changing Environment: Proceedings Of The British Hydrological Society International Conference, Exeter, July 1998*, Volume 1, 33–42.

Kirby, C., Newson, M.D., and Gilman, K. (Editors), 1991. *Plynlimon Research: The First Two Decades*, Report No. 109, Institute Of Hydrology, Wallingford, UK.

Lamb, R.L., 1999. Calibration of a conceptual rainfall-runoff model for flood frequency estimation by continuous simulation, *Water Resour. Res.* **35**, 3103–3114.

Lettenmaier, D.P. and Gan, T.Y., 1990. Hydrological sensitivities of the Sacramento-San Joaquin river basin, California, to global warming. *Water Resour. Res.* **26**, 69–86.

Morris, E.M., 1980. Forecasting flood flows in grassy and forested basins using a deterministic distributed mathematical model. *IAHS Publication* **29**, 247–265.

Naden, P.S., Crooks, S.M. and Broadhurst, P., 1996. Impact of climate and land use change on the flood response of large catchments. *Proc. 31st MAFF Conference of River and Coastal Engineers*, Keele, UK, July 1996, 2.1.1–2.1.16.

Nash, J.E. and Sutcliffe, J.V., 1970. River flow forecasting through conceptual models 1. A discussion of principles. *J. Hydrol.* **10**, 282–290.

NERC, 1975. *Flood Studies Report*, London.

Panagoulia, D. and Dimou, G., 1997. Sensitivity of flood events to global climate change, *J. Hydrol.* **191**, 208–222.

Pilling, C., Wilby, R.L. and Jones, J.A.A., 1998. Downscaling of catchment hydrometeorology from GCM output using airflow indices in upland Wales, in: H. Wheater and C. Kirby (eds), *Hydrology In A Changing Environment: Proceedings Of The British Hydrological Society International Conference, Exeter, July 1998*, Volume 1, 191–208.

Quinn, P.F. and Beven, K.J., 1993. Spatial and temporal predictions of soil moisture dynamics, runoff, variable source areas and evapotranspiration for Plynlimon, Mid-Wales, *Hydrol. Process.* **7**, 425–448.

Quinn, P.F., Beven, K, Chevalier, P. and Planchon, O., 1991. The prediction of hillslope flow paths for distributed hydrological modelling using digital terrain models, *Hydrol. Process.* **5**, 59–79.

Quinn, P., Beven, K.J. and Lamb, R., 1995. The ln (a/tan β) index: how to calculate it and how to use it within the TOPMODEL framework, *Hydrol. Process.* **9**, 161–182.

Sklash, M.G., Beven, K.J., Gilman, K. and Darling, W.G., 1996. Isotope studies of pipeflow at Plynlimon, Wales, U.K., *Hydrol. Process.* **10**, 921–944.

Thompson, N., Barrie, I.A. and Ayles, M., 1981. The Meteorological Office rainfall and evaporation calculation system MORECS. *Hydrological Memorandum No. 45*, U.K Meteorological Office.

Wigley, T.M.L. and Raper, S.C.B., 1992. Implications for climate and sea level of revised IPCC emissions scenarios, *Nature* **357**, 293–300.

Wolock, D.M. and Hornberger, G.M., 1991. Hydrological effects of changes in levels of atmospheric carbon dioxide, *J. Forecasting* **10**, 105–116.